Applied Thermal Engineering 140 (2018) 580–592

Contents lists available at ScienceDirect

Applied Thermal Engineering

journal homepage: www.elsevier.com/locate/apthermeng

Research Paper

Parametrized analysis of a carbon dioxide transcritical Rankine cycle driven by solar energy

Cristóbal Sarmiento[a], José M. Cardemil[a,*], Andrés J. Díaz[b], Rodrigo Barraza[c]

[a] Mechanical Engineering Department, Universidad de Chile, Beauchef 851, Santiago, Chile
[b] School of Industrial Engineering, Universidad Diego Portales, Santiago, Chile
[c] Mechanical Engineering Department, Universidad Técnica Federico Santa María, Santiago, Chile

HIGHLIGHTS

- A detailed model of the system is presented considering mass, energy, exergy, and heat transfer analysis.
- An exergoeconomic analysis is used as a figure of merit to optimize the system configuration.
- A multiobjective optimization is used to evaluate the trade-off between exergy efficiency and thermoeconomic cost.
- The presence of a regenerator increases considerably the energetic and economic benefit.
- Incorporating a solar source changes the optimum design in transcritical Rankine cycles.

ARTICLE INFO

Keywords:
Supercritical CO_2
Transcritical Rankine cycle
Solar energy
Thermoeconomic analysis

ABSTRACT

Several authors have reported in the literature the benefits of transcritical carbon dioxide regenerative Rankine power cycles using low - and medium - temperature sources. However, their technical potential when driven by solar-thermal collectors has not been fully addressed yet. The methodology presented herein is based on two parametric analyses: the first approach attempts to determine the heat transfer area of the regenerator and its respective cost, and the second approach studies the radial heat transfer in each solar collector, at different operation pressures, aiming to determine the heat losses, the pressure drop and the overall performance of the collectors with the use of supercritical Carbon Dioxide. Therefore, through this analysis, the total area required by each component is determined. Then, the solar field configuration is optimized to maximize the exergy efficiency. In that sense, by considering the differences of the specific costs for each area, a multi-objective optimization methodology is applied to the cycle, which determines the best configuration and operation pressure for the cycle based on exergy destruction minimization and the minimum thermoeconomic cost. These results allow determining an optimum size design for the regenerator and solar field configuration, which takes full advantage of the available energy at the lowest possible cost.

1. Introduction

During recent decades, the world energy demand and the CO_2 concentration in the atmosphere have increased considerably [1], encouraging engineers and scientists to promote the utilization of renewable resources.

In this context, solar energy has received large attention due to its high availability and widespread distribution [2,3]. Here, Concentrated Solar Power (CSP) has been singled out as the most appropriate technology for the achievement of a large share of renewable energy production, due to its ease of integration with storage [4–6]. Among the CSP technologies, Parabolic Trough Collectors (PTC) coupled to a thermal cycle (i.e., Rankine or Brayton) are considered the most mature technology, since they have been commercially available since 1982, and represent more than 80% of the CSP installed capacity worldwide [5].

Although the accumulated experience of CSP technologies, researchers continue seeking the implementation of novel techniques for improving their performance and increasing their conversion efficiencies [4]. For instance, most of the CSP-PTC plants in operation use synthetic oil as the Heat Transfer Fluid (HTF) in the solar field, which interacts with a steam generator through a heat exchanger. The use of synthetic oil restricts the cycle temperature to approximately 400 °C, since the oil degrades at higher temperatures, which increases the

* Corresponding author.
E-mail address: jcardemil@ing.uchile.cl (J.M. Cardemil).

https://doi.org/10.1016/j.applthermaleng.2018.04.097
Received 7 December 2017; Received in revised form 9 April 2018; Accepted 20 April 2018
Available online 22 April 2018
1359-4311/

Nomenclature

A	area (m^2)
a_1,a_2,a_3	solar collector's performance coefficients
B_1,B_2	coefficients for F_{BM} correlation
c	specific cost per unit of transferred exergy ($\$_{USD}$/kWh)
C_{bare}	reference bare cost (ev. in 2011) ($\$_{USD}$)
$\dot{C}$	cost rate ($\$_{USD}$/h)
c_p	specific heat (kJ/kg K)
D	hydraulic diameter (m)
E	energy (kJ)
f	friction factor
F_{BM}	bare module factor
F_p	working pressure factor
h	specific enthalpy (kJ/kg)
h_c	convective heat transfer coefficient (kW/m^2 K)
HCE	heat collection element
$\dot{I}$	capital investment rate ($\$_{USD}$/h)
k	conductivity (kW/m K)
$\dot{m}$	mas flow rate (kg/s)
N_{loop}	number of loops in the solar field
Nu	Nusselt number
P	pressure (MPa)
Pr	Prandtl number
$\dot{q}$	heat transfer rate per unit of length (kW/m)
$\dot{Q}$	heat transfer rate (kW)
Re	Reynolds number
s	specific entropy (kJ/kg K)
$\dot{S}_b$	incident solar beam radiation (W/m^2)
T	temperature (K)
U	global heat transfer coefficient (kW/m^2 K)
V	velocity (m/s)
$\dot{W}$	work rate (kW)
x_1,x_3,x_3	coefficients for C_{bare} correlation
y_1,y_2,y_3	coefficients for F_p correlation
Z	size parameter

Greek symbols

α	fraction of the maximum power
ΔL	longitudinal section of the solar collector (m)
ΔP	pressure drop (Pa)
η	efficiency
μ	dynamic viscosity (kg/m s)
ξ	effectiveness
ρ	density (kg/m^3)
ψ	specific exergy (kJ/kg)
$\dot{\Psi}$	exergy rate (kW)

Subscripts

amb	ambient
ave	average
b	bulk
cv	control volume
col	collector
cond	conductive
conv	convective
CO_2	Carbon Dioxide
dest	destruction
ex	exergy
high	high pressure
loss	lost
low	low pressure
o	death state
op	optical
q	heat transfer
rad	radiative
reg	regenerator
s	sun
SF	solar field
sol	solar
SunAbs	solar irradiation absorption
u	useful
W	water
wall	wall side

maintenance cost and environmental risks [4]. Some of the solutions for these shortcomings correspond to the so-called "*Direct Steam Generation*" (DSG) system, and the use of either molten salts or CO_2 as the HTF. Direct steam generation considers the flow of water directly into the absorber tubes of the parabolic trough collectors, generating steam as it flows through the solar field [7]. This configuration shows several benefits and improves conversion efficiency up to 23% (solar to electricity) [8]. The main drawback of DSG is constituted by the thermo-mechanic stresses concentrated in the absorber tube, due to the phase change process and the different heat capacities of each phase flowing inside the tube [4].

Molten salts are already being used as thermal storage medium [9]. However, the use of molten salts requires the implementation of a complex control scheme in order to prevent solidification, which occurs close to 250 °C [9].

The use of CO_2 as the HTF in the solar field has been widely proposed due to its chemical stability and low critical temperature (31.1 °C, 7.38 MPa) [10–15]. In addition, CO_2 can be used directly as the working fluid in the thermal cycle [13,14,16–20], removing the need for a heat exchanger between the solar field and the power cycle, reducing the capital cost of the installation and reaching an outstanding thermodynamic performance for regenerative Rankine cycles. However, s-CO_2 cycles also have some drawbacks due to the high operating pressures, which demand strong walls on the vessels, increasing the material costs [16]. Furthermore, the integration of Thermal Energy Storage (TES) with CO_2 has not been solved yet. For this reason, several authors [19,21–23] have proposed concrete sensible TES, a cheap and simple solution for DSG and s-CO_2 cycles.

Carbon dioxide was a widely used HTF for refrigeration applications until the 1900s, most of its thermos-physical properties are broadly known [24]. Later, new synthetic heat transfer fluids were employed, such as CFCs and HFCs, which show excellent performance in thermal cycles. Nonetheless, several authors have indicated that these fluids are harmful to the environment in terms of ozone depletion and/or global warming potential [25]. Other fluids have been proposed as alternative for thermal cycles, such as ammonia or hydrocarbon mixtures, but they have been shown to be highly toxic and inflammable, respectively [26]. Hence, during the last decade, CO_2 has been reconsidered as a working fluid, because of its comparative advantages [26], which comprise:

- Non-flammable.
- Non-toxic.
- Environment-friendly (zero ozone depletion potential and low global warming potential) [27].
- Highly available.
- Non-corrosive.

In addition, several studies in the literature have also noted the high potential of using CO_2 in cycles of medium and low temperatures sources [17,26,28–32] to achieve high conversion efficiencies with low physical footprint associated to the operation of thermal cycles. In particular, the use of CO_2 as a working fluid in solar collectors was originally proposed by Zhang and Yamaguchi [10,33]. They conducted an experimental study on evacuated-tube flat-plate solar collectors, using supercritical CO_2 as working fluid directly in the absorber tube. The authors concluded that, during the tests, the time-weighted daily average collector efficiency is approximately 50% higher than that found in collectors that use water as working fluid.

The use of CO_2 as working fluid in thermal cycles has been intensively analyzed in recent years, pointing out that the future research pathways to system components should consider operating parameter optimizations, and control strategies [13]. Although, there is no supercritical CO_2 Rankine cycle in operation up to now, it is becoming a future pathway due to its promising features. For large scale and high temperature, it is already demonstrated that the recompression layout is the most efficient, but for smaller scales and mid to high temperature the best configuration depends on the specific feature of the application. As CO_2 cycle performance can vary depending on the layout configuration, further studies on layouts are required to design better performing cycles [14].

Regarding the performance assessment and economic evaluation of CO_2 power cycles, Cayer et al. [28] developed a parametric analysis of a transcritical Rankine cycle with and without a regenerator, using waste heat as energy source. The authors developed a methodology for determining the total heat transfer area of the heat exchangers considering different operating conditions. Due to the highly variable thermos-physical properties of CO_2, which do not allow applying conventional methods, they proposed a discretization methodology for analyzing the heat exchangers. That methodology was later implemented for comparing the performance of CO_2 cycles against other fluids commonly used in Organic Rankine Cycles, showing that the CO_2 cycle achieves the highest exergy efficiency within the mid temperature region (150–400 °C) [26]. In addition, that approach also allowed to develop an optimization framework for such cycles, considering desing and operation variables [30]. Nevertheless, the aforementioned studies only consider a constant heat source to determine the optimal design for s-CO_2 cycles.

Concerning the use of supercritical Carbon Dioxide (s-CO_2) in CSP plants, Chapman and Arias [16] developed an assessment of a s-CO_2 Brayton cycle using parabolic trough collectors that was compared with the current CSP technology that uses Therminol VP1 as the HTF. The authors affirmed that the pumping power of both cycles is similar. Additionally, s-CO_2 simplifies the cycle, since it allows for a reduction on the size of the turbomachinery and decreases the deterioration of the solar field absorber tubes. The authors, however, only considered one loop of the series collector and did not consider other configurations to assess the best performance of the solar field. Recently, a comprehensive analysis of CO_2 cycles powered by parabolic trough collectors was developed by Passos et al. [34], where the tradeoffs observed in CSP plants when the solar collector's efficiency is accounted for system's overall efficiency were revealed. In that context, the selection of a Rankine over a Brayton cycle strongly depends on the operating parameters imposed to the cycle, specifically, on the temperature and pressure at the collector's inlet. Considering that such conditions are highly influenced by the characteristics of the regenerator it results clear that such effect should be further study. Even though these last two studies present an interesting approach for the integration of s-CO_2 cycles with CSP technology, they do not allow establishing the optimal system design, considering costs and thermodynamic performance (energy and exergy).

Regarding the PTC modeling procedure, a complete and deep methodology was proposed in 2003 by Forristal [35], who developed a computational model of three types of PTCs using synthetic oils and water as HTF. The model results were validated against Dudley's test results [36] for an LS-2 collector, and they showed less than 2% error. Hence, this theoretical modeling allows for the determination of the detailed behavior of a PTC and its performance under different operating conditions. However, this analysis only considers incompressible liquid as HTFs at low pressure. It constitutes the theoretical basis for implementing an analysis for assessment of s-CO_2 as HTF in parabolic trough collectors. In addition, Padilla et al. [37] further developed a theoretical model of a PTC, defining a detailed methodology for conducting exergy analysis on a PTC, which evaluates different types of exergy losses occurring in the PTC and identifies sources of irreversibilities to optimize the operating conditions.

Considering the environmental impact associated to the operation of thermal systems, CO_2 constitutes an interesting candidate for innovative cycles and energy conversion technologies and offers a concrete and sustainable solution for the growing world energy demand. The recent literature shows that CO_2 has excellent potential as HTF in cycles driven by solar energy. In addition, CSP technologies, especially parabolic trough collectors, are mature enough to be adapted for coupling with s-CO_2 cycles. Nevertheless, the integration of a PTC solar field in a regenerative Rankine cycle implies a deep assessment about the energy potential utilization, since the heat source (solar in this case) varies its thermal performance as function of the pressure and temperature of the inlet HTF. In that sense, the idea of incorporating both technologies implies a new evaluation of the configurations proposed in the literature that seek to find the best configuration for a solar PTC field using s-CO_2 as working fluid. In that context, this work aims to assess the performance of a CO_2 transcritical Rankine cycle, using solar energy as the heat source and considering the flow of CO_2 directly into the absorber tube. Therefore, it proposes adapting some of the current evaluation methodologies in an optimization model for dealing with CO_2 transcritical cycles by using parabolic trough collectors, considering different solar field's configurations. As shown in the following sections, the configuration is optimized in terms of size of the solar field, size of heat exchanger and operation pressure, maximizing the exergy efficiency and minimizing the exergy costs of the produced energy.

2. System description

The regenerative Rankine cycle analyzed herein consists of a steam turbine, a regenerator, a heat source, a condenser and a circulation pump. The cycle considers a PTC solar field as the heat source, where s-CO_2 flows directly though the solar field. The heated CO_2 is delivered to the turbine, where its expansion produces work. The CO_2 discharged at the turbine's outlet is still at high temperature, and it then passes to the regenerator, where heat is transferred to the CO_2 flow before it enters the solar field, taking advantage of the waste heat. The cold CO_2 is then condensed and pumped back to the solar field, as shown in Fig. 1.

Coolant water enters the cold side of the condenser at 25 °C. To ensure that the temperature of the hot and cold side of the condenser do not cross, the pinch point between the inlet CO_2 on the hot side and the outlet water on the cold side is set to 5 °C ($T_{W,out} = T_6 - 5$ °C).

Commonly, CO_2 Rankine cycles are analyzed by considering a constant heat source modeled as a boiler or a heat exchanger at fixed working conditions [26,28–30]. This work aims to analyze the use of solar energy as an energy source, and thus, the inlet heat to the system varies depending on the solar field's inlet temperature. However, since the objective of this work is to analyze the trends of design considerations for the cycle, the solar radiation is considered constant at 1000 W/m^2. Yet, the nominal inlet temperature to the solar field depends directly on the regenerator's size. For this reason, the size of the regenerator has a direct influence on the amount of energy entering the system, and its effect on the cycle's efficiency is addressed.

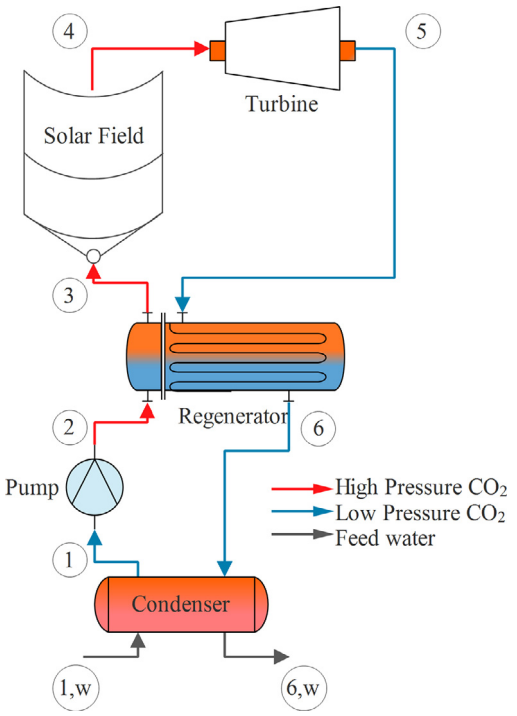

Fig. 1. Solar driven CO_2 power cycle.

3. Methodology

The present work attempts to identify the best cycle's configuration, aiming to achieve high levels of utilization of the solar source, minimizing the system costs. The regenerator improves the exergy efficiency of the system, recovering waste heat at the turbine's outlet, to increase the solar field's inlet temperature. But, on the other hand, the solar field decreases its thermal performance as the inlet temperature increases, inducing several inefficiencies in the collectors, due to the rise of thermal losses on the absorber tube. In that sense, it is necessary to properly assess the influence of regenerator's size in the thermal efficiency of the solar field. Therefore, the analysis proposed herein attempts to determine the best size relation in terms of the regenerator's total area and the solar field aperture area, due to the competing effects produced by these two components and the high costs related to them. In addition, the effect of cycle's high pressure is also analyzed, due to its influence on the cost of the equipment and on the energy balance of the turbomachinery.

Considering the aforementioned effects, the present work proposes using the total heat transfer area (considering the heat exchanger and the collectors) to size and compare each component in discussion. To do so, two parametric analyses are performed: one regarded the heat exchanger configuration, and the other took into consideration the features of the solar field composed of parabolic trough collectors. The exergy efficiency is proposed as the figure of merit to quantify the performance of the cycle and identify the rationale for the use of the energy resource, as suggested in [26,29].

The simulation of the system is developed in three stages. The first stage consists of energy and exergy analyses of each component. In the second stage, a parametric analysis of the regenerator and the solar field is applied to assess performance with s-CO_2 use. Finally, it is conducted an economic analysis of the regenerator and the solar field, in function of the total area of each one. Thus, a thermodynamic model is developed, considering several commonly used assumptions as listed below, and suggested in [26,28–30]:

- No appreciable variations of kinetic and potential energies are expected.
- The cycle is assumed to strictly operate under steady state conditions.
- The pressure drop through the heat exchangers is neglected.
- Both turbomachinery devices are assumed to operate at constant isentropic efficiencies of 0.8 for each device.
- The effectiveness of the condenser is assumed constant and equal to 0.9.
- The CO_2 exits the condenser as saturated liquid at 25 °C.
- The mass flow rate flowing through the solar field is fixed at 10 kg/s to facilitate the escalation of the results.

Table 1
Collector characteristics.

Parameter	Value
Parabolic trough type	LS-3
Heat Collection Element (HCE) length	4.06 (m)
HCE per solar collector	8
Collector aperture	5.59 (m)
Absorber tube diameter	0.066 (m)
Absorber tube coating	Black Chrome
Absorber material	B42 Copper
Annulus gas	Air
Pressure in absorber annulus	1.0E − 09 (torr)

The simulations are carried out considering two configurations of the Rankine cycle: with and without a regenerator. Each heat exchanger is considered as counter-flow, the regenerator effectiveness, the solar field size and the pump's outlet pressure, are varied in the analysis to determine the best configuration among them, aiming to maximize the exergy efficiency of the system and minimize the cycle's costs.

The main features of the solar field are listed in Table 1 and illustrated in Fig. 2, and the environmental conditions are defined for a solar irradiance of 1000 W/m^2, an ambient temperature of 25 °C and an atmospheric pressure of 1 atm.

3.1. Energy analysis

The energy analysis is based on the first law of thermodynamics, which applies for all the components and the whole cycle. Thermal losses are considered only in the PTC modeling, while the other components are considered as adiabatic. Therefore, the energy balance is defined as follows:

$$\frac{dE_{cv}}{dt} = \dot{Q} - \dot{W}_{cv} + \sum_{i}^{n} \dot{m}_i h_i - \sum_{e}^{n} \dot{m}_e h_e \quad (1)$$

where $\dot{Q}$ is the heat transfer rate, $\dot{W}_{cv}$ is the work transfer, h is the specific flow enthalpy and $\dot{m}$ is the mass flow rate. The subscripts i and e denote the inlet and exit of the system, respectively. Since the model considers steady state conditions, the variation in time of the total energy rate, dE_{cv}/dt , is neglected.

3.2. Exergy analysis

Exergy represents quantitatively the maximum theoretical work obtainable from an overall system, which consists of the system itself and the environment, as the system reaches equilibrium with the environment (death state). Hence, exergy is the useful energy or potential for producing work by a system. Exergy is destroyed partially or totally in proportion to the entropy generated by the system, which is associated to its irreversibilities [38]. Thus, an exergy analysis recognizes underperforming devices and shows possible solutions for improving the utilization of available resources. The relation between exergy changes and exergy destruction is indicated by the second law of thermodynamics, which is the basis of this modeling [39]. The exergy

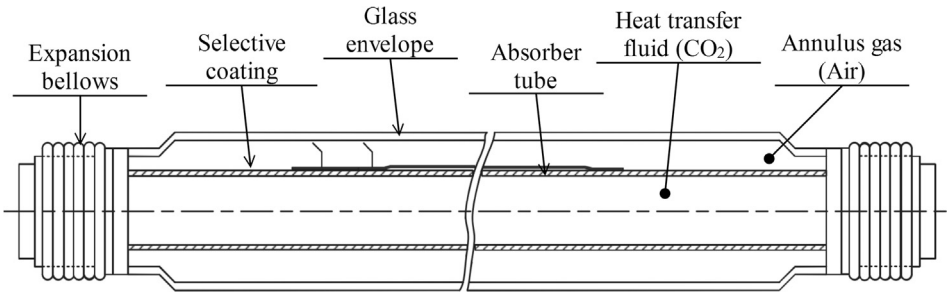

Fig. 2. Diagram of the heat collection element.
Adapted from [37].

balance for each device analyzed herein is defined as:

$$\frac{d\Psi_{cv}}{dt} = \sum_{j}^{n} \dot{\Psi}_{q,j} - \dot{W}_{cv} + \sum_{i}^{n} \dot{m}_i \psi_i - \sum_{e}^{n} \dot{m}_e \psi_e - \dot{\Psi}_{dest} - \dot{\Psi}_{loss} \tag{2}$$

where $\dot{m}_i$ is the inlet mass flow rate, $\dot{m}_e$ is the exit mass flow rate, ψ is the specific flow exergy, and $\dot{\Psi}$ is the exergy rate. The subscripts *loss* and *dest* denote whether exergy is lost or destroyed, respectively. In this work, the exergy losses are due to heat transfer losses to and from the absorber tube due to the environment and collector's optical error. In the same way, the destroyed exergy considers the exergy destruction by the friction viscous forces on the HTF and the heat transfer, from high to low temperatures, between the components of the absorber tube. The model considers a steady state condition. Finally, the exergy rate related to heat transfer $\dot{\Psi}_{q,j}$ is defined as:

$$\dot{\Psi}_{q,j} = \left(1 - \frac{T_o}{T_j}\right)\dot{Q}_j \tag{3}$$

where T_o represents the temperature of the death state, T_j is the temperature of the element j of the system and $\dot{Q}_j$ is the heat transfer rate between the element and the surroundings. The specific flow exergy is defined by the following expression:

$$\psi_f = h - h_o - T_o(s - s_o) \tag{4}$$

where h is the specific enthalpy, s is the specific entropy and the subscript o refers to the death state. Thus, the useful exergy rate in an energy conversion device is defined as:

$$\dot{\Psi}_u = \dot{m}(\psi_e - \psi_i) \tag{5}$$

which accounts for the maximum useful work that the device can deliver.

Several authors have proposed different expressions for defining the exergy available in incident solar radiation over a surface. However, the most common expression was established by Petela [40], who treated the exergy as equivalent to the maximum energy transferred by the propagation, in a non-participant medium, of electromagnetic waves emitted by a black body, which depends on the temperature of the source. Thus, considering the heat transfer between the sun and solar collector's surface, the following equation holds:

$$\dot{\Psi}_{sol} = \dot{S}_b A_{SF}\left(1 - \frac{4}{3}\left(\frac{T_o}{T_s}\right) + \frac{1}{3}\left(\frac{T_o}{T_s}\right)^4\right) \tag{6}$$

where $\dot{S}_b$ is the incident solar beam radiation, A_{SF} is the solar field collecting area and T_s is the temperature of the sun, assumed as a black body at 5778 K.

From the aforementioned definitions, the exergy efficiency of a solar collection element and the complete solar field is determined by the ratio of the useful exergy and the exergy delivered by the solar radiation:

$$\eta_{ex} = \frac{\dot{\Psi}_u}{\dot{\Psi}_{sol}} \tag{7}$$

The performance of the cycle is computed by the exergy efficiency, defined as the ratio between the actual work delivered (exergy) and the exergy available from solar radiation.

$$\eta_{ex;Cycle} = \frac{\dot{W}_u}{\dot{\Psi}_{sol}} \tag{8}$$

The exergy efficiency performs an essential role as figure of merit in this report. It is applied to either a component or the entire system, and it represents how the system exploits the energy potential available (with respect to the death state). Unlike energy efficiency, which only shows the proportion of energy benefit over the inverted energy, an exergy analysis for each component reveals the points at which the most share of entropy is generated. Thus, efforts to improve the weaknesses of the system can be better focused.

3.3. Regenerator parametric analysis

The regenerator parametric analysis considers the regenerator as a counter-flow heat exchanger and determines the global heat transfer capacitance (UA) and the global heat transfer coefficient (U).

3.3.1. Assessment of the global heat transfer capacitance

Modeling heat exchangers using incompressible working fluids is a simple task based on energy balances. However, more considerations are required for s-CO_2 due to its low critical temperature, which induces several variations of its thermos-physical properties, such as heat capacity. That high variation on the specific heat prevents the analysis of heat exchangers using such conventional methods as NTU or LMTD. For this reason, a parametric analysis is developed, as suggested in [26,28]. The analysis considers a physical discretization of heat exchangers, stating a minimum of 25 partitions for assessment of regenerator's thermal conductance. The specific heat of CO_2 in each partition is considered constant. Then, by applying an energy balance, the total heat exchange rate and the inlet and outlet enthalpies are determined. Finally, the numeric value of the heat transferred from one stream to the other is divided according to the amount of partitions considered for the heat exchanger by using the following expression:

$$\dot{Q}_{reg,i} = \dot{m}_{CO_2}(h_{in} - h_{out}) \tag{9}$$

where $\dot{Q}_{reg,i}$ is the heat exchanged in each partition. Enthalpies are evaluated at the inlet and outlet conditions of each partition. Considering the amount of heat exchanged within the discretized domain, the global heat transfer coefficient is determined by using the inlet and outlet temperatures as boundary conditions and applying the logarithmic mean temperature difference method for a counter-flow configuration [41], as follows:

$$UA_i = \frac{\dot{Q}_{reg,i}}{\left(\frac{(T_{hot,out} - T_{cold,in}) - (T_{hot,in} - T_{cold,out})}{ln\left(\frac{T_{hot,out} - T_{cold,in}}{T_{hot,in} - T_{cold,out}}\right)}\right)} \tag{10}$$

where UA_i is the global heat transfer coefficient of each partition i and T is the temperature. The subscripts *hot*, *cold*, *in* and *out* denote hot and cold streams on inlet or outlet conditions, respectively. Finally, the global capacitance of the regenerator is estimated as the sum of the capacitance in each partition:

$$UA_{reg} = \sum_{i=1}^{n} UA_i \tag{11}$$

3.3.2. Global heat transfer coefficient

The global heat transfer coefficient is estimated considering different heat transfer correlations for the high pressure and the low pressure streams, as suggested by Cayer et al. [28]. The low pressure superheated stream from the turbine is analyzed considering Petukhov's correlation [41], which states that the forced convection heat transfer coefficient of single phase CO_2 at low pressures, flowing in turbulent flow regime is defined as follows:

$$U_{low,i} = \frac{k_{CO_2}}{D}\left(\frac{(f/8)RePr_{ave}}{12.7\sqrt{f/8}\,((Pr_{ave}^{2/3})-1) + 1.07}\right) \tag{12}$$

where $U_{low,i}$ is the heat transfer coefficient per unit area in a segment i, k_{CO_2} the conductivity of CO_2, D the section diameter, Pr_{ave} the average Prandtl number, Re the Reynolds number and f the friction factor, defined as:

$$f = (1.82log_{10}(Re)-1.64)^{-2} \tag{13}$$

Krasnoshchekov-Protopopov's correlation [42], which assumes that CO_2 flows in the turbulent regime at supercritical pressures, is considered for the high pressure stream:

$$U_{high,i} = \frac{k_{CO_2}}{D}\left(\frac{(f/8)RePr_{ave}}{12.7\sqrt{f/8}\,((Pr_{ave}^{2/3})-1) + 1.07}\left(\frac{\mu_b}{\mu_{wall}}\right)^{0.11}\left(\frac{k_b}{k_{wall}}\right)^{-0.33}\left(\frac{c_{P_{ave}}}{c_{P_b}}\right)^{0.35}\right) \tag{14}$$

where $U_{high,i}$ is the heat transfer coefficient per unit area in a segment i, k is the thermal conductivity, μ is the dynamic viscosity, and c_p is the specific heat of CO_2. The subscripts *wall* and *b* refer to the heat exchanger wall and the fluid bulk, respectively. Krasnoshchekov-Protopopov's correlation holds as a correction of Petukhov's correlation, considering the differences in the thermos-physical properties between the bulk fluid and the wall. Finally, the total heat transfer area of the regenerator is determined by the following equation:

$$\frac{1}{UA_i} = \left(\frac{1}{U_{high,CO_2}A_{high,CO_2}} + \frac{1}{U_{lowCO_2}A_{low,CO_2}}\right)_i \tag{15}$$

where U is the heat transfer area in segment i. A_{high,CO_2} and A_{low,CO_2} are the heat transfer area of the high and low pressure sides of the regenerator, respectively. The values of A_{high,CO_2} and A_{low,CO_2} are considered equivalent, as if they are two concentric tubes.

3.4. Parabolic trough collector using supercritical carbon dioxide

The behavior of the solar collector is usually described by the thermal efficiency of the collection device. This efficiency is the ratio between the useful heat delivered by the collector and the incident solar radiation [43]. Since that ratio is highly dependent on the operating conditions, the efficiency is commonly correlated to the ambient and inlet temperatures. For parabolic trough collectors, the efficiency is commonly stated by a correlation that depends on the collector geometry, working fluid thermos-physical properties and the construction materials of the absorber tube, as follows:

$$\eta_{col} = \eta_{op} - a_1(T_{in}-T_{amb}) - a_2\frac{(T_{in}-T_{amb})}{\dot{S}_b} - a_3\frac{(T_{in}-T_{amb})^2}{\dot{S}_b} \tag{16}$$

where η_{op} is the collector optical efficiency a, b and c are correlation coefficients associated with thermal losses and $\dot{S}_b$ is the solar irradiance.

The use of s-CO_2 in parabolic trough collectors and the effect of the variable thermos-physical properties on collector's efficiency have not been reported in the literature. Thus, in order to conduct a deep analysis of the complete cycle, a detailed heat transfer model for the PTC is developed by adapting an existing model to assess its behavior using s-CO_2 as working fluid. The theoretical model developed by Forristall [35] for incompressible liquids is considered. It incorporates calculations for the heat transfer interactions between the surfaces, elements composing the absorber tube and the ambient. Additionally, several correlations from the literature are taken into consideration to estimate the heat transfer coefficient of the forced convection inside the tube and the natural convection outside the glass envelope, as well as the radiation heat transfer and the heat conduction through the brackets supporting the absorber within the trough. Hence, with these models, the details of all heat transfer gradients inside the absorber tube and heat losses to the ambient environment are determined. Forristall's model is adapted in order to account for the main features of using s-CO_2 as working fluid, instead of incompressible fluids. This heat transfer model considers the interaction of several components, as described in Figs. 3a and 3b.

The model shown in Fig. 3a consists in an analytical approach that allows assessing the heat transfer between the different layers for a unitary longitudinal section. Hence, the radial energy balance for a longitudinal section shorter than the length of an absorber tube is defined as follows:

$$\dot{q}_{12conv} = \dot{q}_{23cond} \tag{17}$$

$$\dot{q}_{3SunAbs} - \dot{q}_{23cond} - \dot{q}_{34conv} - \dot{q}_{34rad} - \dot{q}_{cond;braquet} = 0 \tag{18}$$

$$\dot{q}_{45cond} = \dot{q}_{34conv} - \dot{q}_{34rad} \tag{19}$$

$$\dot{q}_{5SunAbs} + \dot{q}_{45cond} = \dot{q}_{56conv} + \dot{q}_{57rad} \tag{20}$$

$$\dot{q}_{HeatLoss} = \dot{q}_{56conv} + \dot{q}_{57rad} + \dot{q}_{cond;braquet} \tag{21}$$

where $\dot{q}_{12conv}$ is the convection heat transfer between the HTF and the absorber tube, $\dot{q}_{23cond}$ is the conduction heat transfer between the absorber tube inner surface and the outer surface, $\dot{q}_{3SunAbs}$ is the solar irradiation absorption in the absorber, $\dot{q}_{34conv}$ is the convection heat transfer between the absorber tube and the glass envelope, $\dot{q}_{34rad}$ is the radiation heat transfer between the absorber tube and the glass envelope, $\dot{q}_{45cond}$ is the conduction heat transfer between the glass envelope inner surface and outer surface, $\dot{q}_{5SunAbs}$ is the solar irradiation

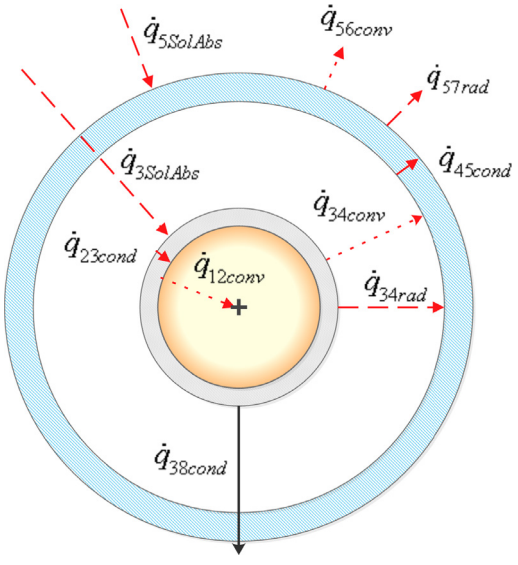

Fig. 3a. 1D Energy balance, adapted from Forristal [35].

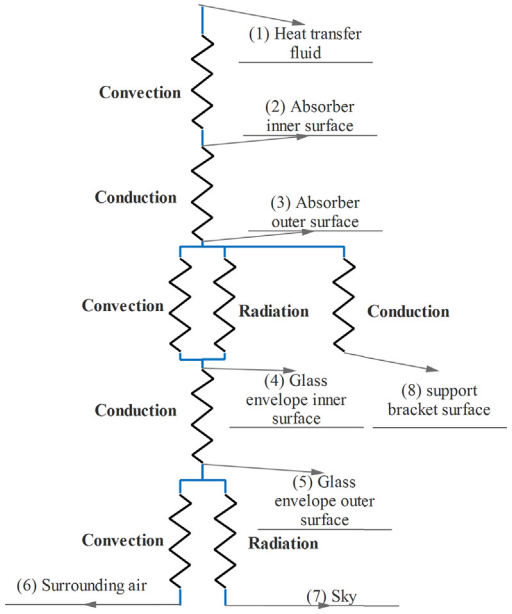

Fig. 3b. Thermal resistance model, adapted from Forristal [35].

absorption in the glass envelope, $\dot{q}_{56conv}$ is the convection heat transfer from the glass envelope to the atmosphere, $\dot{q}_{57rad}$ is the radiation heat transfer between the glass envelope and the sky, $\dot{q}_{cond;braquet}$ is the heat loss through the support bracket and $\dot{q}_{HeatLoss}$ is the total heat loss from the solar collector section.

As mentioned above, the heat transfer model between the working fluid and the absorber tube inner surface is adapted to account for the particular features of s-CO_2. The model is based on the basic equation for convection,

$$\dot{q}_{12conv} = \pi D_2 h_{c1}(T_2 - T_1) \tag{22}$$

where D_2 is the absorber inner diameter and T is the fluid temperature. The subscripts 1 and 2 refer to the average of the HTF and the inner surface of the absorber tube, respectively (see Fig. 3b). h_1 is the convection heat transfer coefficient, evaluated considering the Krasnoshchekov-Protopopov's correlation for the Nusselt number, suggested for forced convective heat transfer at supercritical conditions [42].

$$Nu = \left(\frac{(f/8)Re_{D_2}Pr_{ave}}{12.7\sqrt{f/8}\,((Pr_{ave}^{2/3})-1) + 1.07} \left(\frac{\mu_1}{\mu_2}\right)^{0.11} \left(\frac{k_1}{k_2}\right)^{-0.33} \left(\frac{c_{p_{ave}}}{c_{p_1}}\right)^{0.35} \right) \tag{23}$$

where f is the friction factor defined in Eq. (13) and Re is the Reynolds number of the flow in the absorber tube.

The pressure drop of the flowing CO_2 in the absorber tube is estimated by the following equation, which applies for horizontal pipes and fully developed turbulent flow [44]:

$$\Delta P = \frac{f \Delta L V_{ave}^2}{2 D_2 \rho_{ave}} \tag{24}$$

where ΔP is the pressure drop in the longitudinal section, V_{ave} is the average flow velocity, ρ_{ave} is the average HTF density and ΔL is the length of the longitudinal section.

3.5. Thermoeconomic analysis

To conduct an equivalent comparison between the area of the solar field and the regenerator size, an economic analysis based on the thermoeconomic cost is performed. Thermoeconomics is the branch of engineering that appropriately combines, at the level of system components, exergy based thermodynamic evaluations and economic principles. That approach provides useful insights for the design and operating cost-effective systems [45]. The cost function depends on the parameters of interest, whereas the specific component cost is expressed as function of the thermodynamic design parameters. The cost balance is written for each equipment k in terms of the flow cost rate ($\$_{USD}$/h) as:

$$\sum_{in} \dot{C}_{in,k} + \dot{I}_k = \sum_{out} \dot{C}_{out,k} + \dot{C}_{w,k} \tag{25}$$

where $\dot{I}_k$ is the capital investment in cost per time unit, and the subscripts *in* and *out* refers to the cost rates which enters and exits from the system, respectively. In particular,

$$\dot{C}_k = c_k \dot{\Psi}_k \tag{26}$$

where $\dot{c}_k$ is the specific cost per unit of transferred exergy and $\dot{\Psi}_k$ is the exergy rate at point k.

3.5.1. Economic modeling

Due to the difficulties in obtaining reliable information about the equipment costs, the analysis is developed through purchase cost correlations for each component. For instance, the cost of the regenerator, the condenser, the turbine and the pump are estimated with the methodology proposed by Turton [46], which estimates the cost for each cycle's component as function of a size parameter, type of construction, materials, working pressure and device configuration. The size parameter of each component is a characteristic feature of the device, such as the total heat transfer area for a heat exchanger and the shaft power for a pump. Thus, it assesses lumped economic figures of the devices. The correlation derived in 2011 states that the component purchase cost per unit of size is corrected by the working pressure and material, as follows:

$$Cost_{2011} = C_{bare} F_{BM} \tag{27}$$

where C_{bare} is the reference cost of the equipment in US dollars (evaluated in 2011) and F_{BM} is the bare module factor. The latter factor corrects the cost by considering the influence of the construction materials and the working conditions of the system's component. The cost is correlated by the size of the equipment (Z) according to the following equation:

$$\log_{10} C_{bare} = x_1 + x_2 \log_{10} Z + x_3 (\log_{10} Z)^2 \tag{28}$$

where the parameters x_j are correlation coefficients, which are specific to each type of component. The bare module factor is defined as:

$$F_{BM} = (B_1 + B_2 F_M F_P) \tag{29}$$

where the parameters B_i are correlation coefficients for the component type and working conditions, F_M is a factor related to the construction material and F_P is a factor related to the working pressure, which adheres the following relation:

$$\log_{10} F_P = y_1 + y_2 \log_{10} P + y_3 (\log_{10} P)^2 \tag{30}$$

where the parameters y_i the coefficients for heat exchanger type and P is the working pressure in bar. All the coefficients and parameters aforementioned are listed in [46].

The purchase cost of each cycle device (pump, turbine and heat exchangers) in 2011, estimated through the correlations listed above, is updated to the present cost using the Chemical Engineering Plant Cost Index (CEPCI) [47].

The cost of the solar field is estimated based on the specific cost of the collector (unitary area) reported in the literature and related to currently operating parabolic trough plants [48], $\$_{USD}$ 170/m^2.

4. Simulation model

The system is modeled using Engineering Equation Solver (EES) [49]. This software, which is widely used by the scientific community for macroscopic thermodynamic simulations [26,28,29], not only

solves algebraic equations governing the cycles, but also easily communicates with a thermos-physical properties database based on REFPROP-NIST [50]. As mentioned, the solar field is based on the model developed by Forristal [35], yet in order to enable the possibility of assessing a significant number of configurations (e.g. loops, number of heat collection element per loop, operating pressures and regenerator effectiveness) a surrogate model (response surface approximation model) is built for mapping the performance in such configurations. This approach is a very efficient method for reducing the intrinsic computational time of optimization techniques and complex thermal system simulations [51].

There are several methods to create surrogate models (i.e., polynomial, kriging, neural networks, and support vector machines). However, there is no common opinion as to which method performs better than the others, since the performance of the approximation depends on the nature of the problem. In the present study, a linear interpolation method is chosen, as suggested in [52]. Using such method, the surrogate models are built, configuring functions in the form $v = f(x_1,x_2)$.

4.1. Validation

The results are validated by comparing against the results presented in the literature. The simulation model of a regenerator using s-CO_2 is contrasted with the results presented by Cayer [28] for a supercritical Rankine cycle using s-CO_2 as working fluid. Table 2 summarizes the validation procedure. In Cayer's work, α is a parameter that defines the fraction of the maximum power output, defined by the Carnot efficiency. The main difference between the two models is the calculation of the heat exchanger area. The model presented by Cayer considered a number of fins in the heat exchanger's shell but did not specify the number. However, the differences between the results are satisfactory for validating the model, since the total area of the regenerator heat exchanger is compared.

Regarding the solar collector model, the test results presented by Dudley [36] for a LS-2 solar collector are considered. The main characteristics of the collector tested are equivalent to those listed in Table 1. Yet, the environmental conditions for the test are fixed at 850 W/m^2 and 22 °C. The comparison between the test results and the model shows a satisfactory goodness of fit, with a coefficient of determination of 0.998. This value indicates that the proportion of the variance predicted from the model is 99%. In other words, the proposed model explains 99% of the cases for temperatures from 0 to 350 °C.

Finally, the pressure drop reached at the solar field differs in 10.31% of the value presented by Chapman and Arias [16] for a s-CO2 solar collector loop. The difference is produced because the detailed information about the geometry of the collector unions is not available.

5. Results and discussion

The aim of the methodology presented in the previous section is to determine the optimal configuration for the cycle, in terms of the regenerator size and the total area of the solar field that maximizes the exergy efficiency of the cycle, while minimizing the thermoeconomic cost. However, since the solar field modifies its behavior significantly according to its configuration and operating conditions, the procedure requires performing a deep analysis in this regard. The analysis reveals the existence of an optimal configuration for the solar field, in terms of the arrangement of the solar collectors in parallel rows (denominated loops) and the number of collectors that constitutes each loop (i.e., in series). Hence, this analysis identifies the conditions that reduce the exergy destruction by pressure drops and exergy losses by heat transfer to the environment.

The first approach of the analysis is devoted to the performance characterization for a single solar heat collection element (HCE) exposed to different operation conditions, which covers most of the possible configurations of the solar field and optimizes its distribution. The assessment aims to maximize the exergy delivered by the solar collector and applies the methodology for exergy assessment of parabolic trough collectors developed by Padilla et al. [37].

Table 2
Validation results of regenerator's model.

Specific net power output (kW/kg)					
P_{High} (MPa)	α	Regenerator	Present work	Reference	Error (%)
11.5	0.15	No	18.78	18.80	0.01
Heat exchanger coefficient (kW/K)					
11.54	0.15	No	3357	3361	0.13
11.58	0.20	No	4724	4727	0.06
Heat exchanger area (m^2)					
11.46	0.15	Yes	1409	1458	3.48
11.54	0.20	No	993	862.5	7.58

5.1. Single collector parametric analysis

In order to evaluate the influence of the solar field configuration on the system performance, the behavior of a single solar collector using CO_2 as HTF is investigated. The process considered assessing the thermal efficiency and the pressure drop in collector's absorber tube for a longitudinal partition of 1 m, under different operating conditions (temperature and pressure) and different configurations for a specific aperture area. The solar irradiance is assumed constant at 1000 W/m^2 and the mass flow rate through the complete field is fixed at 10 kg/s, which is divided according the number of loops considered. Fig. 4 shows the thermal efficiency of a single solar collector as a function of the inlet temperature and the mass flow rate, which depends on the loops that constitute the solar arrangement.

The shape of the curve observed in Fig. 4 is similar to the thermal efficiency depicted by the collector, using other well-known HTFs. The decrease on the efficiency as the inlet temperature increases is due to the rise in the thermal losses to the environment. In addition, the high temperature of the working fluid reduces the temperature difference with respect to the absorber tube, decreasing the heat transfer rate from the absorber tube to the s-CO_2 flowing inside the tube. In that sense, a lower mass flow rate in the absorber tube induces an increase in the temperature, intensifying the aforementioned phenomena.

On the other hand, increasing the number of loops in the solar field reduces considerably the pressure drop in the absorber tube (Fig. 4). This reduction is not significant for more than four divisions of the mass flow rate. Therefore, more than four loops are not necessary since they do not contribute significantly to reduce exergy losses. As such, it is possible to state the existence of an optimum configuration that maximizes the exergy delivered by the solar field for a specific aperture area.

5.2. Solar field configuration analysis and optimization

The behavior of the solar field considering the modified configurations is analyzed, aiming to analyze the effect on the exergy efficiency for different aperture areas. The number of HCE is varied from 8 to 400, while the inlet temperature ranged from 30 °C to 450 °C.

The solar field is modeled as an open system, for which the inlet exergy is composed of two parts: the exergy of the pressurized CO_2 inlet (preheated by the regenerator) and the exergy associated with the incident solar radiation, given by Petela's equation.

To determine the effect of varying the inlet temperature, the collection area and the number of loops on the solar field exergy efficiency and the variation on the exergy losses are studied. That exergy loss is associated to the heat transfer process between the sun and the working fluid. In that sense, it is necessary to distinguish the types of exergy

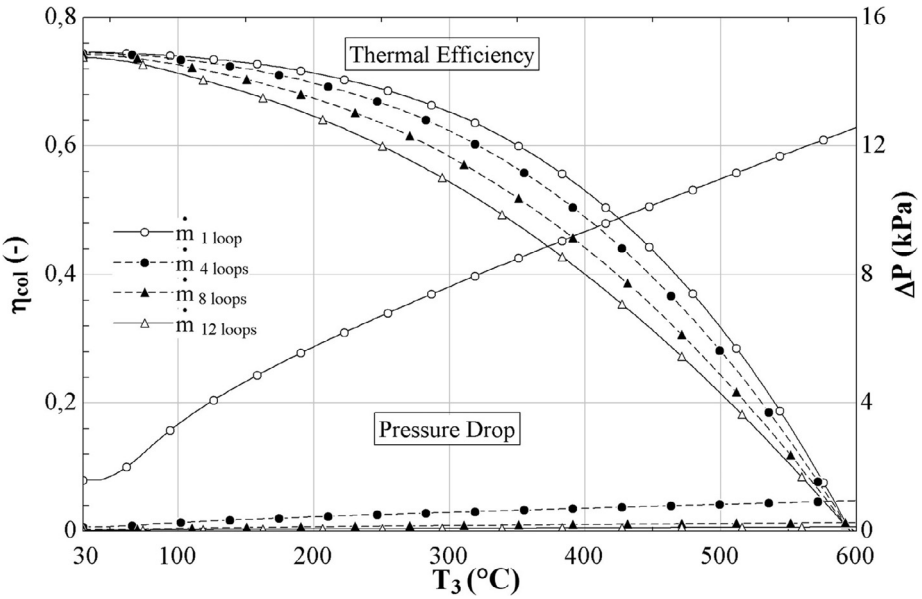

Fig. 4. Thermal efficiency and pressure drop of a single collector of 8 HCE at 15 MPa.

losses considered in this analysis, which consists of all the possible forms of heat transfer observed in the control volume:

- The exergy loss associated to optical errors or alignments at the solar collector.
- Entropy generation due to the heat transfer between the glass envelope and the inner wall of the absorber tube.
- The exergy loss associated to heat losses to the environment.
- The exergy loss due to the pressure drop inside the absorber tube.

The first three processes listed above are inherent to the construction materials of the heat collection device. Therefore, the analysis is focused on minimizing the last two losses, which depend on the operating conditions and the distribution of collectors within the solar field. In this context, Fig. 5 shows the effect of the number of loops on the exergy efficiency of a solar field with 250 HCE operating at an inlet temperature of 250 °C. As explained in the previous section, the pressure drop can be reduced considerably without increasing significantly the number of loops. For this case, the solar field reaches the maximum exergy efficiency at the third loop, and the efficiency decreases linearly for higher numbers of loops. This effect is due to the influence of two factors, shown simultaneously in the figure. The pressure drop reaches values close to zero and then the rate of decrease stagnates, such that it does not represent an additional exergy benefit beyond a particular number of loops. The collector area is fixed, and the increase in the number of loops decreases the number of HCE per row, causing a decrease in the outlet temperature field and consequently the output exergy of the solar field. Such a drop in the outlet exergy induces the slight fall shown by the exergy efficiency curve before the third loop. For this reason, it is possible to affirm the existence of a number of loops that maximizes the exergy efficiency of the solar field.

Fig. 6 shows the results of the parametric analysis described above applied to the complete domain – solar field aperture area and inlet temperature. Each value of exergy efficiency considers the best configuration for the number of solar HCE, taking advantage of the solar resource and establishing the configurations considered for the optimization of the cycle described in the following sections. The maximum exergy efficiency is achieved at a small aperture area. This is because each additional HCE in the field adds its inherent thermal losses, but at the same time increases the inlet solar exergy to the field. For this

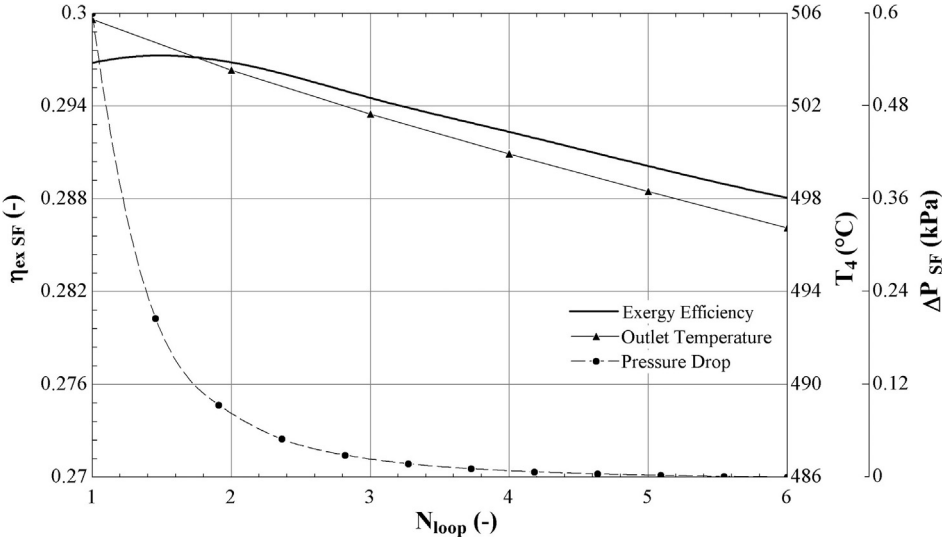

Fig. 5. Exergy efficiency, pressure drop and heat losses of a solar field with 250 HCE and an inlet temperature of 250 °C, at 15 MPa.

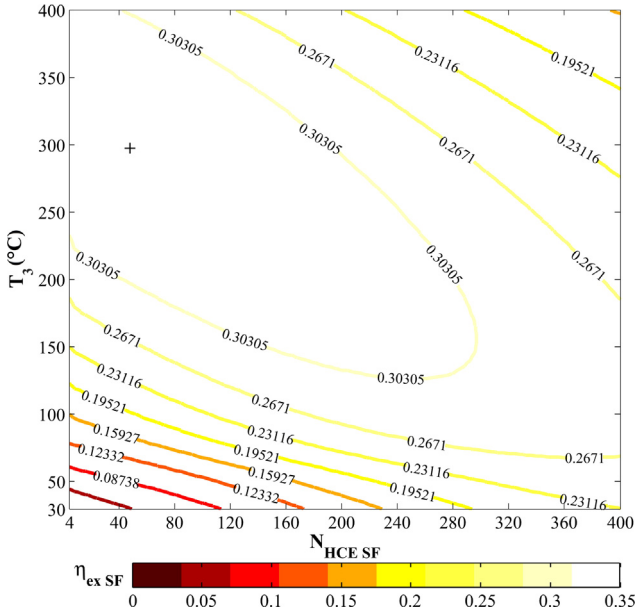

Fig. 6. Maximum exergy efficiency of the solar field as a function of the temperature and the solar field size.

reason, the temperature that maximizes the exergy efficiency of each field size decreases as the number of collectors increases. Thus, it is reasonable to consider a lower inlet temperature for larger aperture areas and higher temperatures for smaller numbers of HCE.

Fig. 7 builds on the results shown in Fig. 6, displaying the temperatures that maximize the exergy efficiency for each solar field's size. As mentioned above, the inlet temperature has a direct relationship with the exergy efficiency: the inlet temperature depends linearly on the field size, and the optimum efficiency values increase for smaller collecting areas. In that sense, from an exergy viewpoint, it is logical to consider a bigger regenerator, which increases the inlet temperature for a small solar field. Similar behavior is observed for higher operating pressures, but leading to better efficiencies and costs. This issue is addressed in the next section through multi-objective optimization, which takes into account the above-mentioned relation between the solar field performance and the regenerator size, as well as the operating pressure and capital costs of the equipment.

5.3. Multi-objective optimization

To find the best design conditions for the solar field aperture area and the regenerator size, a multi-objective optimization is performed. For the system considered herein, the proposed optimization attempts to find an optimum system's configuration, evaluating two objectives at the same time: maximize the exergy efficiency of the system and minimize the thermoeconomic cost of the energy delivered.

Other authors [26,28–30] have proposed the total heat transfer coefficient *UA* as a measure for the size of the heat exchanger used in organic Rankine cycles, considering constant temperature heat sources. However, this measure is not suitable when comparing two different types of components, such as the regenerator and the solar field. Ahmadi et al. [53] proposed applying the weighted sum of objective functions as an optimization methodology, generating a map with the optimum points derived by varying the specific weight given for each objective function, forming a Pareto's frontier with all the best possible cases. This multi-objective methodology provides a visualization of the impact on the thermoeconomic costs of the exergy efficiency and other parameters of interest for the system design. Thus, the optimization methodology considers two objective functions: The first aimed to minimize the thermoeconomic cost related to the energy delivered by the system. The second objective function attempts to maximize the exergy efficiency of the cycle. Both functions depend on design parameters as presented as follows:

$$\begin{aligned} \max f &= \eta_{ex,cycle}(\xi_{reg}, N_{col}, P_{high}) \\ \min g &= \dot{C}_e(\xi_{reg}, N_{col}, P_{high}) \end{aligned} \tag{31}$$

where N_{col} is the number of solar HCE composing the solar field, P_{high} is the highest pressure on the system, and ξ_{reg} is the regenerator effectiveness, which is associated with the regenerator total area. The domain analyzed considered $\xi_{reg} \in [0,1]$, $P_{high} \in [10,20]$MPa, and $N_{col} \in [130,400]$.

Considering the thermoeconomic cost of the energy delivered and the exergy efficiency for each configuration of solar field and regenerator, a direct optimization procedure is applied using a linear search. Fig. 8 shows the relation between those variables, for different configurations in terms of the size of the solar field and the regenerator. The high pressure in this figure is kept constant at 15 MPa. Each curve represents the trade-off between the exergetic efficiency and the thermoeconomic cost, for a fixed regenerator's effectiveness; and for a

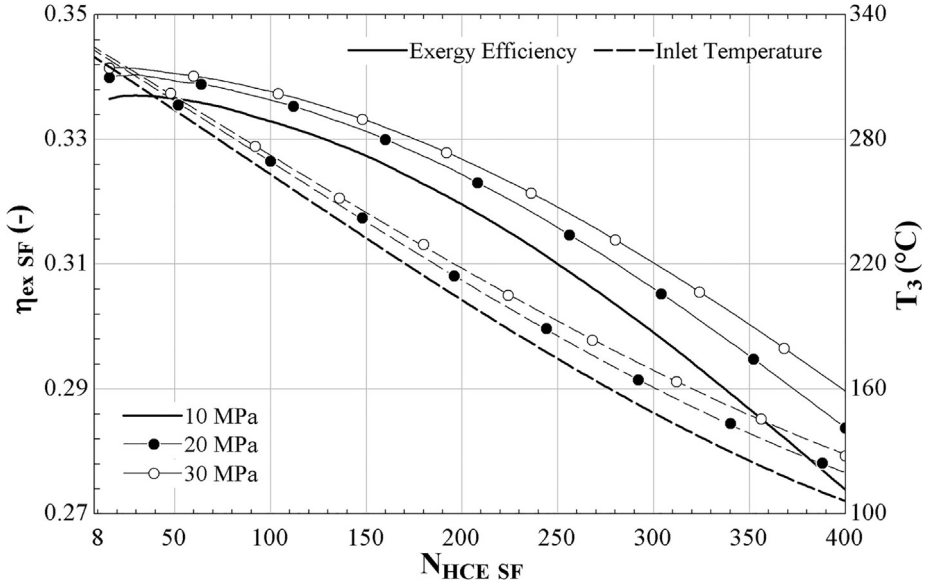

Fig. 7. Optimum inlet temperature for maximization of solar field's exergy efficiency.

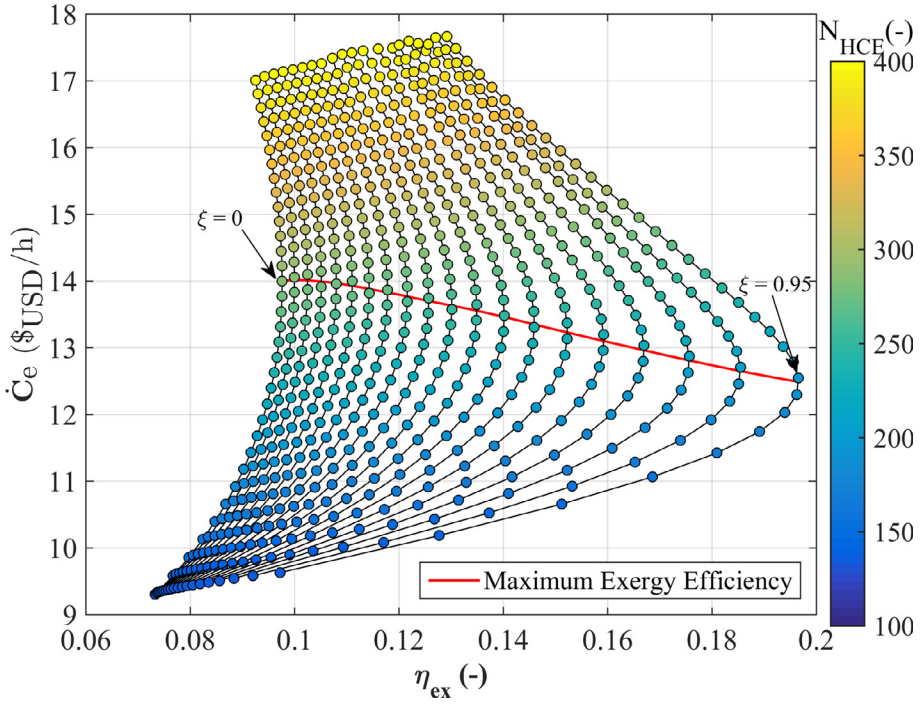

Fig. 8. Pareto frontier for trade-off values for exergy efficiency and the total cost functions for system with a regenerator.

range between 100 and 400 heat collection elements (HCE). By comparing the curves depicted in Fig. 8, it is possible to observe the influence of the regenerator presence in the exergy delivered by the cycle. The way of exploiting energy resources can be improved considerably without a substantial increase in the size of the solar field, by improving the regenerator. Hence, the exergy efficiency could duplicate its value, even with a solar field 30% smaller, when comparing the best and worst scenarios. Even though the investment cost reaches twice its previous value, the useful work produced increases by 40%, which leads to a significant increment in the exergy efficiency, from 9 to 19%. This difference between the increase in the required collecting area and the benefits in terms of useful work, which is attributed to the regenerator, reducing the heat released to the environment at the condenser, thereby taking advantage of the energetic potential of the CO_2 discharged by the turbine. Based on that, the thermoeconomic cost increases as the exergy efficiency increases, yet improving the effectiveness of the regenerator has a significant impact on reducing the thermoeconomic cost of the energy delivered, for the same level of exergy efficiency. This effect is due to the relative cost that the regenerator represents, compared to the solar field: increasing the regenerator size (and cost) induces a

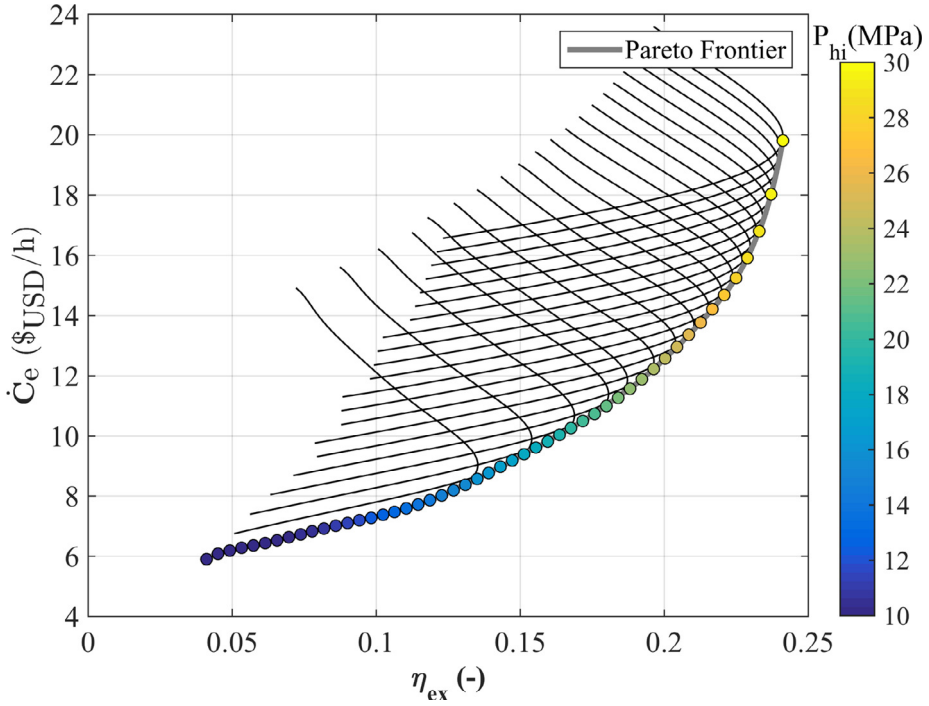

Fig. 9. Pareto frontier for trade-off values for exergy efficiency and thermoeconomic cost for different size of the solar field and operating pressure.

significant improvement on the exergy efficiency and a minor effect on the thermoeconomic cost. The figure also shows that the best exergy efficiency is achieved around 200 HCE, since a further increase on the solar field size induces larger thermal losses and therefore larger exergy losses.

Considering the aforementioned information, the largest size of regenerator is considered for the optimization process, i.e. $\xi_{reg} = 0.95$. Hence, a multi-objective optimization routine is applied for determining the trade-off between the exergy efficiency and the thermoeconomic cost. The process considers a scalar procedure, and a surrogate model as described in the previous section. Fig. 9 shows the results of the optimization routine and the search domain evaluated through the surrogate model. The Pareto frontier is represented by the grey line, as the markers show the pressure that allows achieving that exergy efficiency. It is noteworthy that pressures larger than 30 MPa are not explored, since the increment on the costs are high due to the robustness needed on the equipments, which is also reflected by the shape of the Pareto frontier on Fig. 9. From the figure, it is observed that from 15 to 30 MPa, the exergy efficiency increases from 19.5 to 24.5%, while the thermoeconomic cost increases 7.65 $\$_{USD}$/h. The best solar field configuration increases from 189 to 256 HCE and the net-work produced increases 40%. That relation reflects the compromise between efficiency and cost that the analyst should evaluate during the design process. The optimum configuration of the solar field that configures the Pareto frontier is depicted on Fig. 10. The color map of the curve shows how increases the size of the solar field that allows achieving the best exergy efficiency. That relation allows to assess the compromise between the cost of improving the solar collection area and the effect on the rationality of exploiting resources.

6. Conclusions

The present work describes a parametrical analysis about the behavior of a regenerative Rankine cycle driven by solar energy, using s-CO_2 as working fluid. The analysis is focused on improving the relation between the solar field aperture area, the regenerator size and high pressure, while the exergy efficiency and the thermoeconomic cost of the produced energy are assessed simultaneously. In addition, the cost estimation methodology allows estimating the changes on the capital cost due to changes on the nominal operating conditions, which depends on the operating pressure and material selection (highly influenced by the operating temperature) and design conditions. The proposed multi-objective optimization allowed to determine the best configuration, maximizing the exergy efficiency and reducing the thermoeconomic cost of the energy delivered. Hence, the analysis presents mainly two key findings: first it allows to identify the improvement potential (exergy loss) in every device of the cycle, according to certain operating conditions, and determine the economic value of such losses. Besides that, the exergoeconomic analysis allows determining the configuration that maximizes the benefit, in terms of power delivered and cost, and enabling the evaluation of the compromise between both effects, through pareto fronts.

An exergy-based approach allows the regenerative Rankine cycle to take the maximum advantage of the energy potential from the solar field, which enables a more accurate assessment about the utilization of the available resources. Thus, the regenerator can increase significantly the useful work produced, in comparison with the same cycle without a regenerator. The results show that the regenerator allows to double the exergy efficiency, resulting in 38.21% more useful work produced with a smaller solar field (34.46% smaller). Therefore, the cycle becomes more compact and efficient. That result is due to the fact that the regenerator represents a negligible impact on the cost of the system, compared with the exergetic benefit associated to its function in the system. In that sense, the solar field size has a design limitation, which determines the maximum aperture area, since for larger areas it is not possible to take rational advantage of the resource. The exergy efficiency of the solar field can be improved considerably by modifying the distribution of its collectors as function of the number of loops into which the inlet mass flow is divided. Such changes have direct influence on the destroyed exergy, associated with the pressure drop inside the absorber tube, and the exergy loss to the environment. Both types of exergy losses depend directly on the mass flow rate and the number of heat collection elements in series per loop. The number of loops that maximizes the exergy performance does not exceed four loops for a solar field of s-CO2 and an aperture area of 20 to 400 HCE.

The inlet temperature of the solar field has an optimum value that

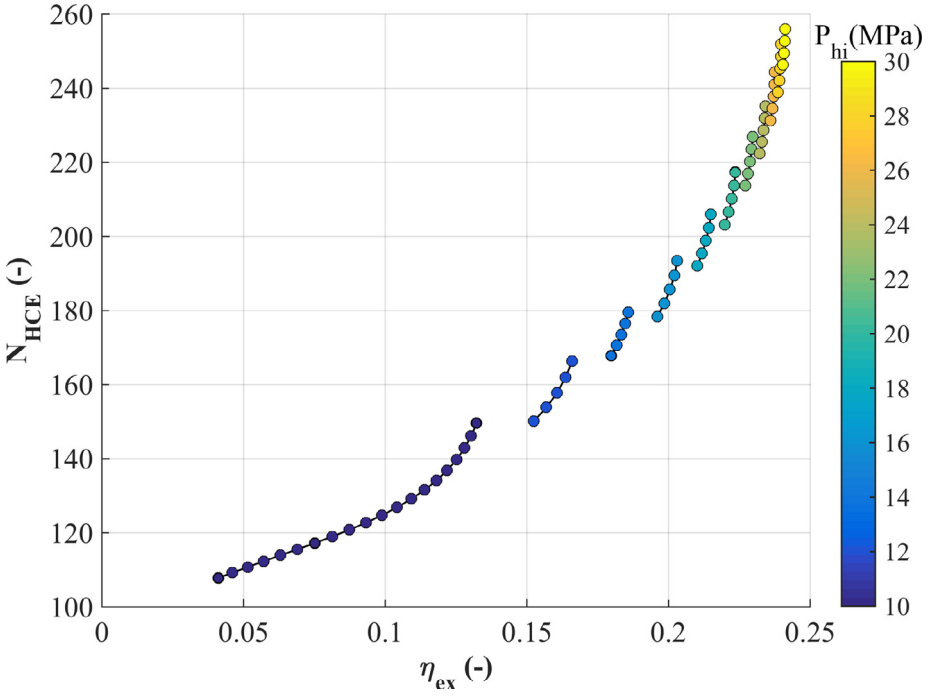

Fig. 10. Best configurations for the size of the solar field and cycle's high pressure, that form the Pareto frontier.

maximizes the exergy efficiency of the solar field. For small fields of 20 solar HCE, the thermal loss associated with the area is smaller, so the field can admit high temperatures (315 °C) without lowering its exergy efficiency. In the same way, solar fields of 400 HCE, with more thermal losses, should use lower temperatures (120 °C). These results provide relevant information for future evaluations regarding thermo-solar cycles that use this novel HTF. In future research, it would be interesting to analyze the transient regime and the integration of TES into s-CO_2 solar cycles, since CO_2 presents some disadvantages due to the high working pressures.

Acknowledgement

The authors wish to express their gratitude for the financial support from CONICYT/FONDAP 15110019 “Solar Energy Research Center“-SERC-Chile and the project Fondecyt N° 11140725 from Chilean CONICYT.

References

[1] The International Energy Agency IEA, Key World Energy, p. 82, 2015.
[2] R. Perez, M. Perez, A fundamental look at energy reserves for the planet, IEA SHC Sol. Updat. 50 (2009) 2–3.
[3] R. Perez, K. Zweibel, T.E. Hoff, Solar power generation in the US: too expensive, or a bargain? Energy Policy 39 (11) (2011) 7290–7297.
[4] A. Fernández-García, E. Zarza, L. Valenzuela, M. Pérez, Parabolic-trough solar collectors and their applications, Renew. Sustain. Energy Rev. 14 (7) (2010) 1695–1721.
[5] IEA, Technology Roadmap Solar Thermal Electricity, Int. Energy Agency, p. 52, 2014.
[6] L.A. Weinstein, J. Loomis, B. Bhatia, D.M. Bierman, E.N. Wang, G. Chen, Concentrating solar power, Chem. Rev. 115 (23) (2015) 12797–12838.
[7] E. Zarza, M.E. Rojas, L. González, J.M. Caballero, F. Rueda, INDITEP: the first pre-commercial DSG solar power plant, Sol. Energy 80 (10) (2006) 1270–1276.
[8] E. Zarza, et al., Direct steam generation in parabolic troughs: final results and conclusions of the DISS project, Energy 29 (5–6) (2004) 635–644.
[9] U. Herrmann, D.W. Kearney, Survey of thermal energy storage for parabolic trough power plants, J. Sol. Energy Eng. 124 (2) (2002) 145.
[10] X.R. Zhang, H. Yamaguchi, D. Uneno, K. Fujima, M. Enomoto, N. Sawada, Analysis of a novel solar energy-powered Rankine cycle for combined power and heat generation using supercritical carbon dioxide, Renew. Energy 31 (12) (Oct. 2006) 1839–1854.
[11] Y. Song, J. Wang, Y. Dai, E. Zhou, Thermodynamic analysis of a transcritical CO2 power cycle driven by solar energy with liquified natural gas as its heat sink, Appl. Energy 92 (Apr. 2012) 194–203.
[12] T. Neises, C. Turchi, A comparison of supercritical carbon dioxide power cycle configurations with an emphasis on CSP applications, Energy Procedia 49 (2013) 1187–1196.
[13] J. Sarkar, Review and future trends of supercritical CO2 Rankine cycle for low-grade heat conversion, Energy 48 (Mar. 2015) 344–351.
[14] Y. Ahn, et al., Review of supercritical CO2 power cycle technology and current status of research and development, Nucl. Eng. Technol. 47 (6) (2015) 647–661.
[15] W.H. Stein, R. Buck, Advanced power cycles for concentrated solar power, Sol. Energy 152 (2017) 91–105.
[16] D. Chapman, D. Arias, An Assessment of the Supercritical Carbon Dioxide Cycle for Use in a Solar Parabolic Trough Power Plant, Supercritical CO_2 Power Cycle Symposium, Troy, New York, April 2009.
[17] G. Shu, L. Shi, H. Tian, S. Deng, X. Li, L. Chang, Configurations selection maps of CO2-based transcritical Rankine cycle (CTRC) for thermal energy management of engine waste heat, Appl. Energy 186 (2017) 423–435.
[18] L. Shi, G. Shu, H. Tian, G. Huang, T. Chen, X. Li, D. Li, Experimental comparison between four CO_2-based transcritical Rankine cycle (CTRC) systems for engine waste heat recovery, Energy Convers. Manag. 150 (August) (2017) 159–171.
[19] G. Shu, X. Li, H. Tian, L. Shi, X. Wang, G. Yu, Design condition and operating strategy analysis of CO2 transcritical waste heat recovery system for engine with variable operating conditions, Energy Convers. Manag. 142 (2017) 188–199.
[20] Y. Chen, Novel cycles using Carbon Dioxide as working fluid: new ways to utilize energy from low – grade heat sources, KTH Industrial Engineering and Management, May 2006.
[21] A. Stückle, D. Laing, H. Müller-Steinhagen, Numerical simulation and experimental analysis of a modular storage system for direct steam generation, Heat Transf. Eng. 35 (9) (Dec. 2013) 812–821.
[22] R. Tamme, D. Laing, W.D. Steinmann, Advanced Thermal Energy Storage Technology for Parabolic Trough, in: Proceedings of International Solar Energy Conference (ISEC), Hawaii, USA, International Solar Energy Conference, March, 2003.
[23] D. Laing, D. Lehmann, C. Bahl, E.Z. Ag, Concrete Storage for Solar Thermal Power Plants and Industrial Process Heat, Renew. Energy (2008) 1–6.
[24] J.A. Lipa, C. Edwards, M.J. Buckingham, Specific heat of CO2 near the critical point*, Phys. Rev. A 15 (2) (Feb. 1977) 778–789.
[25] X.-R. Zhang, H. Yamaguchi, K. Fujima, M. Enomoto, N. Sawada, A feasibility study of CO2 - based Rankine cycle powered by solar energy *, JSME Int. J. 48 (3) (2005) 540–547.
[26] J.M. Cardemil, A.K. Da Silva, Parametrized overview of CO2 power cycles for different operation conditions and configurations - An absolute and relative performance analysis, Appl. Therm. Eng. 100 (2016) 146–154.
[27] J.M. Calm, G.C. Hourahan, Refrigerant data summary, Eng. Syst. 18 (11) (2001) 74–88.
[28] E. Cayer, N. Galanis, M. Desilets, H. Nesreddine, P. Roy, Analysis of a carbon dioxide transcritical power cycle using a low temperature source, Appl. Energy 86 (7–8) (Jul. 2009) 1055–1063.
[29] E. Cayer, N. Galanis, H. Nesreddine, Parametric study and optimization of a transcritical power cycle using a low temperature source, Appl. Energy 87 (4) (Apr. 2010) 1349–1357.
[30] F.G. Battisti, J.M. Cardemil, F.M. Miller, A.K. da Silva, Normalized performance optimization of supercritical, CO2-based power cycles, Energy 82 (2015) 108–118.
[31] F.G. Battisti, J.M. Cardemil, A.K. da Silva, A multivariable optimization of a Brayton power cycle operating with CO2 as working fluid, Energy 112 (2016) 908–916.
[32] F. Crespi, G. Gavagnin, D. Sánchez, G.S. Martínez, Supercritical carbon dioxide cycles for power generation: a review, Appl. Energy 195 (2017) 152–183.
[33] X.R. Zhang, H. Yamaguchi, An experimental study on evacuated tube solar collector using supercritical CO2, Appl. Therm. Eng. 28 (10) (Jul. 2008) 1225–1233.
[34] L.A. de Araujo Passos, S.L. de Abreu, A.K. da Silva, Optimal scale of solar-trough powered plants operating with carbon dioxide, Appl. Therm. Eng. 124 (2017) 1203–1212.
[35] R. Forristall, Heat Transfer Analysis and Modeling of a Parabolic Trough Solar Receiver Implemented in Engineering Equation Solver, National Renewable Energy Laboratory (NREL), Colorado, 2003.
[36] V.E. Dudley, G. Kolb, M. Sloan, D. Kearney, Test Results: SEGS LS-2 Solar Collector, Report of Sandia National Laboratories, 1994.
[37] R.V. Padilla, A. Fontalvo, G. Demirkaya, A. Martinez, A.G. Quiroga, Exergy analysis of parabolic trough solar receiver, Appl. Therm. Eng. 67 (1–2) (2014) 579–586.
[38] A. Bejan, Fundamentals of exergy analysis, entropy generation minimization, and the generation of flow architecture, Int. J. Energy Res. 26 (7) (2002).
[39] M.J. Moran H.N. Shapiro, Fundamentals of engineering thermodynamics, 5th ed., 2006.
[40] R. Petela, Exergy of heat radiation, J. Heat Transfer 86 (2) (1964) 187.
[41] F.P. Incropera, D.P. DeWitt, T.L. Bergman, A.S. Lavine, Fundamentals of Heat and Mass Transfer, John Wiley & Sons, 2007.
[42] I.L. Pioro, H.F. Khartabil, R.B. Duffey, Heat transfer to supercritical fluids flowing in channels — empirical correlations (survey) Atomic Energy of Canada Limited, vol. 230, 2004, pp. 69–91.
[43] J. Duffie, W. Beckman, Solar Engineering of Thermal Processes, 3th ed., John Wiley, New York, USA, 2006.
[44] B.R. Munson, D.F. Young, T.H. Okiishi, Fundamentals Of Fluid Mechanics, 6th Ed., John Wiley and Sons, Inc., 2009.
[45] P. Ahmadi, I. Dincer, M.A. Rosen, Exergy, exergoeconomic and environmental analyses and evolutionary algorithm based multi-objective optimization of combined cycle power plants, Energy 36 (10) (2011) 5886–5898.
[46] R. Turton, R.C. Bailie, W.B. Whiting, J.A. Shaeiwitz, Analysis Synthesis and Design of Chemical Processes, Prentice Hall PTR, New Jersey, 2003.
[47] W.M. Vatavuk, Updating the *CE* Plant Cost Index, Chemical Engineering, Issue 1, January, 2002, pp. 62–70.
[48] P. Kurup, C.S. Turchi, Parabolic Trough Collector Cost Update for the System Advisor Model (SAM), November 2015.
[49] S.A. Klein, F.L. Alvarado, Engineering Equation Solver, Version 10.439, F-Chart Software,Madison, WI, 2013.
[50] E.W. Lemmon, M.L. Huber, M.O. McLinden, Reference fluid thermodynamic and transport properties (REFPROP), NIST standard reference database 23—Version 7. 0, 2002.
[51] L. Magnier, F. Haghighat, Multiobjective optimization of building design using TRNSYS simulations, genetic algorithm, and Artificial Neural Network, Build. Environ. 45 (3) (2010) 739–746.
[52] Y. Jin, A comprehensive survey of fitness approximation in evolutionary computation, Soft Comput. 9 (1) (2005) 3–12.
[53] P. Ahmadi, M.A. Rosen, I. Dincer, Multi-objective exergy-based optimization of a polygeneration energy system using an evolutionary algorithm, Energy 46 (1) (2012) 21–31.